JOURNAL OF GEOPHYSICAL RESEARCH, VOL. 88, NO. B11, PAGES 9500-9512, NOVEMBER 10, 1983

SHOCK COMPRESSION OF SINGLE-CRYSTAL FORSTERITE

J. Peter Watt[1] and Thomas J. Ahrens

Seismological Laboratory, California Institute of Technology

Abstract. Dynamic compression results are reported for single-crystal forsterite loaded along the orthorhombic a and c axes to pressures from 130 to 165 GPa. Hugoniot states for the two axes are well described by a single curve offset to densities 0.15-0.20 g/cm^3 lower than earlier data for single-crystal forsterite shocked along the b axis above 100 GPa. Earlier data of Syono et al. [1981a] show marginal support for similar b-axis behavior in the mixed-phase region from 50 to 92 GPa. Thus shocked forsterite is most compressible in the b direction for the mixed-phase and high-pressure regimes (P>50 GPa). These data represent the highest pressures for which shock properties have been observed to depend on crystal orientation. Theoretical Hugoniots for mixed-oxide and perovskite-structure high-pressure assemblages of forsterite calculated from recent experimental data are virtually identical and agree with the b-axis data. The a- and c-axis data are also consistent with both high-pressure assemblages because uncertainties in equation of state parameters produce a broad range of computed Hugoniots. Our calculated "average" Hugoniot is up to 0.13 g/cm^3 less dense than the preferred theoretical Hugoniots, in agreement with earlier measurements on dense polycrystalline forsterite. Interpolation between the single-crystal forsterite Hugoniots and Hugoniots for fayalite and Fo_{45} gives Fo_{88} Hugoniots bracketing Twin Sisters dunite data not previously well fit by systematics. Release paths are steep for the a and b axes but c-axis release paths are much shallower. Hugoniot elastic limits measured for the a and b axes are in good agreement with previous data of Syono et al.; however, the present data for the a axis reveal a triple wave structure: two deformational shock waves as well as the elastic shock, a feature not previously found. The second shock, with amplitude about 9 GPa and a shock temperature of about 350°K, could perhaps be explained by the forsterite $\alpha \rightarrow \beta$ or γ phase transformation.

Introduction

Magnesium-rich olivines are believed to be the dominant mineral component of the upper mantle. Acquisition of data on the high-pressure behavior of olivines is of great importance for interpreting mantle velocity and density profiles derived from inversion of seismic travel time and normal mode data. Until recently, experimental pressures comparable to those in the lower mantle below 670 km could be reached only in shock-wave studies such as those of Trunin et al. [1965], McQueen et al. [1967], and Ahrens and Petersen [1969] on natural forsterite-rich olivines; McQueen and Marsh [1966] and Ahrens et al. [1971] on synthetic forsterite aggregates of 2-5% porosity; McQueen [1968] and Marsh [1980] on synthetic forsterite aggregates of less than 1% porosity; and Jackson and Ahrens [1979] and Syono et al.[1981a] on synthetic forsterite single crystals. In general, these data at pressures over about 80 GPa were interpreted as consistent with an isochemical mixture of oxides, (Mg,Fe)O (rock salt structure) and SiO_2 (stishovite) [Birch, 1952], although Jeanloz and Ahrens [1977] and Jackson and Ahrens [1979] argue for high-pressure phases of olivines denser than the simple close-packed oxide mixture.

In recent years, this high-pressure region of olivine has become accessible to static compression studies combined with in situ X ray work. Results of Liu [1975, 1976a, b], Ito [1977], Mao et al. [1977], and Sawamoto [1977] demonstrate that at pressures and temperatures relevant to the mantle below 670 km, magnesium-rich olivines, pyroxenes, and garnets transform to mixtures of (Mg,Fe)O and $(Mg,Fe)SiO_3$ (perovskite structure) several percent denser than the isochemical oxides.

Several shock recovery experiments have been performed to seek evidence for formation of this high-pressure perovskite-structure(pv) phase in shocked olivine. Jeanloz et al. [1977] observed formation of glassy regions associated with areas having high dislocation density in single-crystal peridot shocked above 56 GPa and speculated that this glass may have formed upon retransformation of a high-pressure phase upon releasing from peak shock pressure. Jeanloz [1980] undertook optical and electron microscopic and infrared spectroscopic studies of recovery products of single-crystal peridot loaded to pressures up to 76 GPa and found no evidence to support formation of a high-pressure phase. There was extensive plastic deformation but no trace remanent high-pressure phases, shock-induced melting, recrystallization or recovery on unloading. From this result, Jeanloz proposed a crystallographically-based model for the shock behavior of olivine that did not require a reconstructive phase transformation. In the model the olivine crystal could be viewed as sets of nearly hexagonally close-packed sheets of oxygen ions with the hexagonal axis along the olivine orthorhombic a axis and the cations interlayered among the oxygen layers. Shock compression distorts the oxygen layers around the intervening cations and leads to the observed high Hugoniot densities. The model predicts that olivine will be most compressible along the a axis, with lower, but roughly equal, compressibilities for the b and c axes.

[1] Now at Department of Geology, Rensselaer Polytechnic Institute.

Copyright 1983 by the American Geophysical Union.

Paper number 3B1078.
0148-0227/83/003B-1078$05.00

Syono et al. [1981b] carried out transmission electron microscopy, electron diffraction, and chemical work on single-crystal forsterite loaded to pressures between 78 and 92 GPa and found formation of precipitates with MgO composition and glassy regions of about $MgSiO_3$ composition. They interpreted this as either production of $MgSiO_3$ (pv) and MgO at high pressures or as incongruent melting of forsterite to produce MgO crystals and $MgSiO_3$ melt. Jakubith and Seidel [1982] shocked an omphacitic eclogite (58% omphacite, 17% kyanite, 17% garnet and 4% quartz) and, using X ray diffraction on the recovered material, inferred the presence of $MgSiO_3$(pv).

Thus, while the evidence for formation of a high-pressure phase with perovskite structure in shock-compressed olivines is not unambiguous, the available data, combined with static compression results, are fairly compelling. The lower mantle below 670 km may well be dominated by perovskite-structure silicates, although Anderson [1977] and Jeanloz and Thompson [1983] argue that an olivine (spinel)-perovskite transition alone is insufficient to account for the sharpness of the 670 km discontinuity. Jeanloz and Thompson support the presence of a chemical discontinuity as well. Anderson [1970], Anderson et al.[1971], Gaffney and Anderson [1973], Burdick and Anderson [1975], and Butler and Anderson [1978] argue for a lower mantle enriched in silicon relative to the upper mantle, a conclusion supported by results of Watt and Ahrens [1982], based on current high-pressure data.

In this paper, we present results for single-crystal forsterite shock-loaded along the a and c axes to pressures up to 165 GPa. Combining these data with b-axis results of Jackson and Ahrens [1979], we can test the prediction of Jeanloz's [1980] model that olivine should be most compressible along the a axis. We also compare our data to a high-pressure phase Hugoniot calculated from static compression and ultrasonic data on MgO and $MgSiO_3$(pv). We find that a- and c-axis Hugoniots are essentially coincident and displaced to densities 0.15-0.20 g/cm^3 lower than those for the b axis. Data for all three axes are consistent with formation of either a high-pressure mixed-oxide or perovskite-structure assemblage, within the uncertainty in the computed Hugoniots. Our preferred interpretation, however, is formation of a high-pressure assemblage somewhat less dense than mixed oxides or perovskites.

Experimental Details

The experiments were executed in a manner similar to those of Jackson and Ahrens [1979]. Synthetic forsterite single crystals (Union Carbide Corporation, Crystal Products Division) were used with the shock propagation direction along either the orthorhombic a or c axis ($b_o < c_o < a_o$). Sample densities were measured by Archimedes' technique with immersion in toluene. The average density was 3.226 g/cm^3; standard deviation was 0.002 g/cm^3 (6 samples). The samples, 2.8-3.3 mm thick, were lapped to within ±0.002 mm of uniform thickness and mounted on 0.5-mm-thick tantalum driver plates with an array of fused quartz arrival mirrors. Lexan projectiles with 1.5 to 2.5-mm-thick tantalum flyer plates were acceleratated in a two-stage light-gas gun to velocities between 5.3 and 6.3 km/s. Projectile velocities were measured using two 15-ns duration flash x-ray sources and 0.01-μs electronic counters to record the interflash time interval over a path of about 350 mm immediately in front of the stationary target assembly. Accuracy of the projectile velocities was ±0.2% except for shot 090, where triggering errors necessitated the use of much lower precision timing data, resulting in a projectile velocity uncertainty of ±6%. The quartz arrival mirrors were illuminated with a Xenon lamp and observed with a TRW image converter streak camera writing on Royal X film at 30 mm/μs. The streak records were calibrated using a modulated laser beam producing timing marks at 16 2/3 ns intervals on the film. Additional details appear in Jackson and Ahrens [1979] and Jeanloz and Ahrens [1980].

All streak records were scanned with a microphotometer, and arrival mirror reflection cutoffs were used to compute the sample and buffer mirror transit times from linear or quadratic least squares fits to the photometer scans. Corrections were applied for projectile tilt and bowing and for nonlinear streak camera writing rate, as required. These effects are described in detail by Jackson and Ahrens [1979] and Jeanloz and Ahrens [1980]. Sample and buffer shock wave velocities could thus be determined to within 1-2%. Hugoniot and partial release state particle velocities, densities, and pressures were computed using the impedance matching technique and the Riemann integral approximation [Rice et al., 1958; Lyzenga and Ahrens, 1978; Jeanloz and Ahrens,1979]. Equation of state data for tantalum were taken from McQueen et al. [1970] and for fused quartz from Wackerle [1962] and Jackson and Ahrens [1979].

Three experiments were also carried out at low pressures in a single-stage 40-mm propellant gun to study directional variation of the Hugoniot elastic limit (HEL) of forsterite to compare with the extensive low-pressure shock-wave work of Syono et al. [1981a]. Raikes and Ahrens [1979] reported an HEL measurement of single-crystal forsterite shocked along the c axis. In the present work, one sample of forsterite was shocked along the b axis and two along the a axis. The elastic precursor to the shock wave was detected using an inclined mirror mounted on top of the sample. Details of the technique are given by Ahrens et al. [1968, 1971] and Raikes and Ahrens [1979].

Results and Discussion

Table 1 lists the measured sample densities, projectile velocities, and sample and buffer mirror shock wave velocities, as well as the calculated Hugoniot and partial release states for the experiments with shock propagation along the forsterite a and c axes (three shots for each direction). Figure 1 shows sample shock wave velocity, u_s, versus sample particle velocity, u_p. Also included are data of Jackson and Ahrens [1979] for shock propagation along the b axis, the single-crystal forsterite measurements of Syono et al. [1981a] for propagation along all three axes, and dense polycrystalline (porosity < 1%) forsterite data of McQueen [1968] and Marsh [1980] at low particle velocities. The data at particle velocities over 3.5 km/s are well described by straight lines with slopes greater than the straight line fitting the lower velocity data and are conven-

TABLE 1. Single-Crystal Forsterite Shock-Wave Data and Calculated Hugoniot and Partial Release States

Shot	ρ_o, g/cm^3	u_{fp}, km/s	u_s, km/s	u_{sb}, km/s	Hugoniot state u_p, km/s	Hugoniot state P, GPa	Hugoniot state ρ, g/cm^3	Partial release state u_p, km/s	Partial release state P, GPa	Partial release state ρ, g/cm^3
a-axis										
080	3.2234	5.36	10.61	8.53	3.85	131.7	5.059	4.68	88.0	4.686
	(±0.0048)	(±0.01)	(±0.14)	(±0.18)	(±0.01)	(±1.3)	(±0.045)	(±0.11)	(±1.0)	(±0.131)
063	3.2275	5.48	10.74	8.83	3.93	136.3	5.094	4.87	94.8	4.600
	(±0.0046)	(±0.01)	(±0.16)	(±0.22)	(±0.01)	(±1.6)	(±0.059)	(±0.14)	(±1.1)	(±0.191)
071	3.2269	6.08	11.28	9.64	4.35	158.3	5.253	5.38	114.4	4.659
	(±0.0040)	(±0.01)	(±0.28)	(±0.20)	(±0.02)	(±3.1)	(±0.100)	(±0.12)	(±1.8)	(±0.192)
c-axis										
088	3.2268	5.31	10.50	8.89	3.82	129.3	5.071	4.91	96.2	4.289
	(±0.0040)	(±0.01)	(±0.12)	(±0.22)	(±0.01)	(±1.2)	(±0.042)	(±0.14)	(±1.1)	(±0.270)
090	3.2219	5.92	11.55	10.70	4.20	156.4	5.065	6.04	142.4	2.278
	(±0.0042)	(±0.35)	(±0.08)	(±0.12)	(±0.27)	(±10.1)	(±0.188)	(±0.07)	(±3.3)	(±1.366)
097	3.2302	6.28	11.39	10.42	4.49	165.3	5.331	5.87	134.8	4.000
	(±0.0048)	(±0.01)	(±0.19)	(±0.35)	(±0.02)	(±2.1)	(±0.070)	(±0.22)	(±9.7)	(±0.640)

u_{fp} is projectile velocity, u_s sample shock wave velocity, u_{sb} buffer mirror shock-wave velocity, and u_p particle velocity.

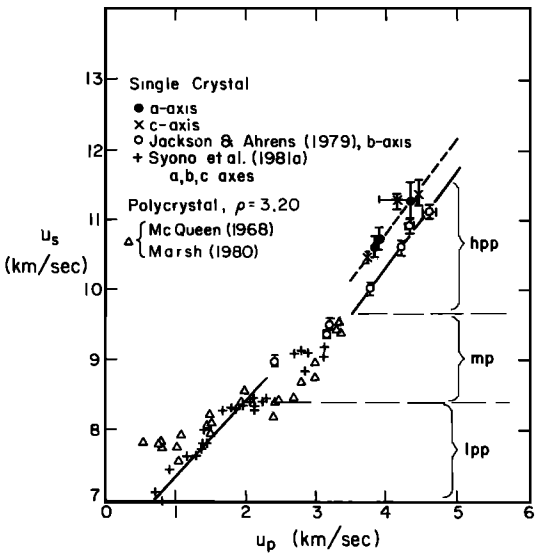

Fig. 1. Forsterite u_s-u_p data for single crystals shocked along the three orthorhombic axes and for dense polycrystals. Low-pressure phase (lpp), mixed-phase (mp), and high-pressure phase (hpp) regions are indicated.

tionally interpreted as representing a high-pressure phase. The a- and c-axis data are displaced to lower particle velocities relative to the b-axis data of Jackson and Ahrens, although slopes of the two straight line segments are the same. A linear least squares fit to the b-axis data gives $u_s = 4.87(\pm2.48) + 1.37(\pm0.18)u_p$ with a correlation coefficient of 0.97 (4 points), while the fit to the combined a- and c-axis data, omitting the uncertain datum at $u_p = 4.20$ km/s (shot 090) is $u_s = 5.60(\pm1.22) + 1.30(\pm0.08)u_p$ with a correlation coefficient of 0.99 (5 data). The line at particle velocities below 2.0 km/s is a linear least squares fit of Syono et al.[1981a] to their single-crystal data. There is no directional dependence evident in these previous data and, accordingly, the sample orientations are not given in the figure (Fig. 2 of Syono et al. distinguishes the three axes).

Figure 2 shows the calculated Hugoniot states for the present a- and c-axis experiments as well as the b-axis data of Jackson and Ahrens [1979], the single crystal data of Syono et al. [1981a] and Raikes and Ahrens [1979], and the dense polycrystal data of McQueen[1968]. The curves are for visual convenience only. The a- and c-axis data offset in Figure 1 produces a displacement of the Hugoniot to lower densities relative to the b-axis Hugoniot. To insure that this difference between the a- and c-axis and b-axis results was not the result of bias in reading the shock-wave records, the streak records for the b-axis experiments reported by Jackson and Ahrens were reanalyzed using the same methods as for the a- and-c axis experiments. Our reanalysis of the b-axis records yielded Hugoniot states in agreement with those determined by Jackson and Ahrens within one standard error, except for the points at 98 and 122 GPa, which agreed within two standard errors. Thus we conclude that at pressures above 100 GPa, single-crystal forsterite is most compressible along the b axis, with lower, but nearly equal,

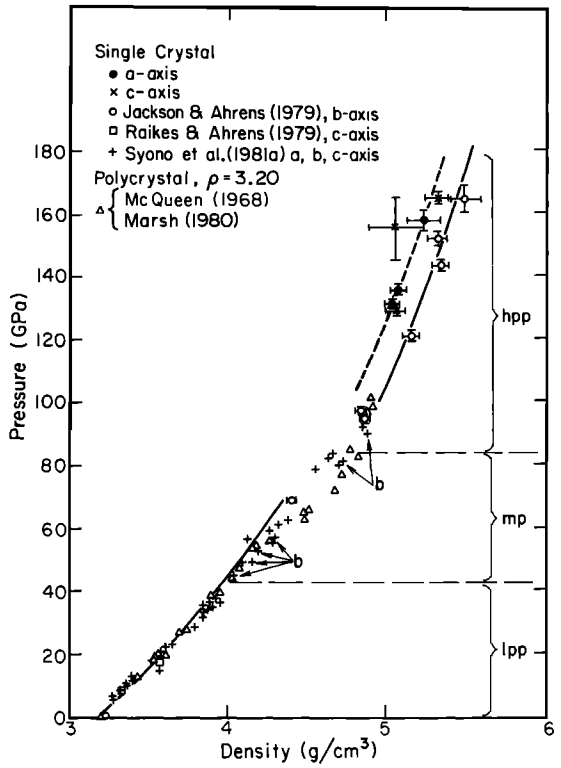

Fig. 2. Hugoniot states for single-crystal forsterite shocked along the three orthorhombic axes and for dense polycrystals in three regimes. The b-axis data of Syono et al.[1981a] are indicated. Greatest compressibilty for the mixed-phase and high-pressure regions occurs along the b axis. Curves are for visual convenience only.

compressibilities for the a and c axes. This disagrees with the crystallographic model of Jeanloz [1980] that predicts highest compressibility for the a axis.

Careful examination of the single-crystal forsterite data of Syono et al. [1981a] to pressures up to 92 GPa provides marginal evidence of directional dependence in agreement with our results. The b-axis data of Syono et al. are indicated in Figure 2 and, in general, lie at densities higher than those reached by the a- and c-axis samples; there is no obvious distinction between the a- and c-axis Hugoniot data. The estimated density error in the data (±1%) is just under twice the width of the plotted crosses, so that the directional dependence is not obvious from their data alone, but taken with our high-pressure results, produce a consistent picture of greater b-axis compressibility above pressures of 50 GPa.

Directional dependence for dynamic properties has been observed earlier in single-crystal calcite, ilmenite, and sodium chloride. Ahrens and Gregson [1964] found that calcite is most compressible when shocked along the trigonal (z) axis to pressures of 25 GPa. Calculation of compressibility $\beta(i)$ along the i axis from single-crystal elastic constant data of Dandekar and Ruoff [1968] gives $\beta(x) = \beta(y) = 2.7 \times 10^{-3}$ GPa^{-1} and $\beta(z) = 8.2 \times 10^{-3}$ GPa^{-1}, in agreement with the shock observation. Thus, the relative compressibilities of the calcite axes persist across the three calcite phase transformations observed in the dynamic experiments. King and Ahrens[1976] observed that single-crystal ilmenite shocked to 70 GPa was most compressible along the trigonal axis, in agreement with static compression data of Liu et al. [1974] for a magnesian ilmenite. Additionally, shock-compression data for single-crystal sodium chloride [Fritz et al., 1971] indicate that the pressure at which the B1-B2 displacive transition occurs under shock varies with shock propagation direction. We note that in calcite and ilmenite, directional dependence occurs throughout the whole pressure range of the experiments, while the forsterite data of Syono et al. [1981a] show no marked dependence on shock propagation direction from the Hugoniot elastic limit to the start of the mixed-phase region around 40 GPa and even beyond.

The present olivine observations represent the highest pressures at which directional dependence of shock properties has been found. At pressures so far above the elastic limit of olivine, 6-13 GPa [Syono et al., 1981a], the hydrostatic approximation should be well satisfied and directional dependence would not be expected. One possible explanation could be sluggish reaction kinetics along the a and c axes compared to the b axis, although again the high pressures make this rather unlikely, and our a- and c-axis data show no evidence for compression approaching the b-axis values, even at 160 GPa. Additional recovery studies similar to that of Syono et al. [1981b] may indicate whether or not the amount of transformation products at a given pressure is direction dependent.

The partial release paths for the a-axis shots (not plotted in Figure 2 for clarity) are steep, and similar to those found by Jackson and Ahrens for the b axis, implying persistence of the high-pressure phase as the samples unload. The c-axis release paths, on the other hand, are much shallower than for the other axes, suggesting more rapid reversion of the high-pressure phase as the samples begin to unload. Thus it seems that there is different behavior upon release from similar Hugoniot states, depending on the axis involved.

We now compare our high-pressure Hugoniot data for olivine with theoretical Hugoniots for mixed-oxide and MgO + $MgSiO_3$(pv) assemblages calculated from ultrasonic, static compression, and Brillouin scattering data. Table 2 lists the equation of state data used for MgO, SiO_2(stishovite), and $MgSiO_3$(pv) and the combined values for oxide and perovskite assemblages. The K_o and $\partial K/\partial P$ data for MgO are the values of Spetzler [1970] as well as recent shock wave and ultrasonic work of Vassiliou and Ahrens [1981] and Jackson and Niesler [1982]. The zero-pressure Grüneisen parameter, γ_o, is that of Anderson and Andreatch [1966]. We assume that the Grüneisen parameter varies with volume as $\gamma/\gamma_o = (\rho_o/\rho)^n$ and take n=1.5, with a large uncertainty (see Davies [1974] for typical values of n for close-packed oxides). The K_o value for stishovite is the average of the tetragonal polycrystalline Hashin-Shtrikman bounds [Watt and Peselnick, 1980] calculated from the Brillouin scattering single-crystal elasticity data of Weidner et al. [1982]. Weidner et al. concluded that their Brillouin data, combined with isothermal hydrostatic compression results, suggest that $\partial K/\partial P$ for stishovite is lower than for other rutile-structure oxides. Ultrasonic values of $\partial K/\partial P$

TABLE 2. Forsterite Equation of State Parameters for Theoretical High-Pressure Phase Hugoniots

	MgO	SiO_2 (stish.)	$MgSiO_3$ (perov.)	2MgO +SiO_2	MgO +$MgSiO_3$
ρ_o, g/cm^3	3.584	4.29	4.10	3.86	3.94
K_o, GPa	163. (±1.)	316. (±1.)	260. (±20.)	211. (±12.)	224. (±12.)
$\partial K/\partial P$, dimensionless	4.1 (±0.2)	4. (±1.)	4. (±1.)	4.1 (±0.5)	4.0 (±0.7)
γ_o, dimensionless	1.54	1.5 (+0.2)	1.0 (±0.5)	1.0 (+0.5)	1.0 (+0.5)
n, dimensionless	1.5	1.5	1.5	1.5 (+0.5)	1.5 (±0.5)
E_{tr}, kJ/g	-	-	-	1.0 (+0.5)	1.0 (±0.5)

for SnO_2, GeO_2 and TiO_2 are 5.13, 6.15 and 6.80, respectively [Chang and Graham, 1975]. Accordingly, we adopt stishovite $\partial K/\partial P$ as 4 ± 1 (see also Bass et al [1981]). The values of ρ_o, K_o, and $\partial K/\partial P$ for $MgSiO_3$(pv) are those due to Yagi et al. [1979a, b]. We calculate zero-pressure properties for oxide and perovskite assemblages from the values for the separate components. The elastic moduli are averaged using the Voigt-Reuss-Hill two-phase average; Hashin-Shtrikman bounds cannot be used because they require the shear moduli of the phases. The oxide and perovskite zero-pressure Grüneisen parameter is found from shock-wave measurements on slightly porous forsterite (R. G. McQueen, personal communication, 1981) to which we assign a large uncertainty. We use the estimate of Jackson and Ahrens [1979] for the transition energy, E_{tr}.

We use third-order finite strain theory and relate isentropes and Hugoniots through the Grüneisen parameter; the complete equations appear in Jackson and Ahrens [1979]. The calculated Hugoniots are shown in Figure 3. The dotted curve at low pressures is the theoretical Hugoniot derived from the ultrasonic forsterite data of Graham and Barsch [1969] and Kumazawa and Anderson [1969], collected in Table 3 of Jackson and Ahrens [1979]. In the high-pressure regime, the dashed curves are theoretical Hugoniots for mixed oxides; the solid curves are for an MgO + $MgSiO_3$ (pv) assemblage. The heavy curves were calculated from the preferred equation of state parameters in Table 2; the light curves include combined uncertainties in all the parameters.

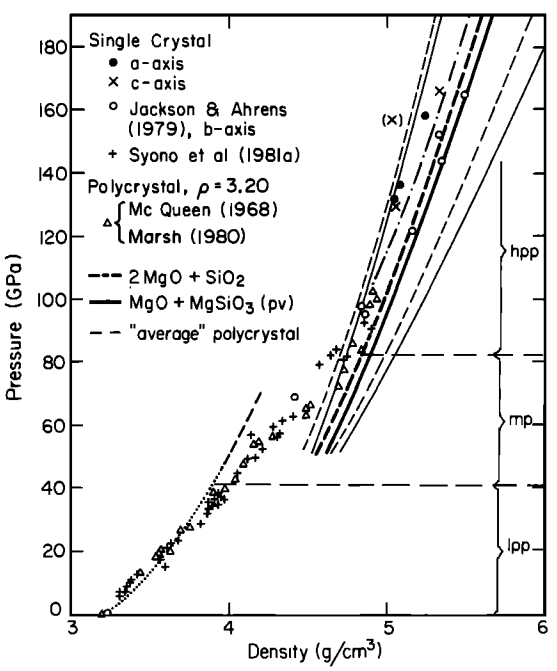

Fig. 3. Calculated Hugoniots for forsterite compared with observed data. In the high-pressure regime, dashed curves are for mixed oxides, solid curves are for a perovskite-structure assemblage. Heavy curves were calculated using the preferred values in Table 2; light curves include combined uncertainties in the equation of state parameters. The "average" curve was calculated using equation (1).

Both the mixed-oxide and the perovskite assemblage preferred high-pressure Hugoniots match the b-axis data of Jackson and Ahrens. In their analysis, Jackson and Ahrens concluded that a mixed-oxide Hugoniot did not lead to sufficiently high densities to account for their data. This was a result of the high values of stishovite $\partial K/\partial P$ (=6) and γ_o (=1.5) used in their analysis.

Jackson and Ahrens treated two possible values for $MgSiO_3$(pv) K_o: an estimate of Liebermann et al. [1977] of 250±30 GPa based on elasticity systematics and a preliminary static compression value of Yagi et al. [1978] of 286±30 GPa. These data led to values of K_o for MgO + $MgSiO_3$(pv) of 219 and 239±20 GPa respectively, compared to the value of 224±12 GPa used here from the refined determination of Yagi et al. [1979b]. The present pv assemblage parameters (Table 2), with lower $\partial K/\partial P$ and γ_o than used by Jackson and Ahrens lead to a preferred hpp Hugoniot about 0.1 g/cm^3 denser than the Jackson and Ahrens Hugoniot with a pv assemblage K_o of 219 GPa and about 0.05 g/cm^3 denser than our mixed-oxide Hugoniot.

The spread in hpp Hugoniot values when all the uncertainties in the equation of state parameters are included is large, even with recent refinements in stishovite and $MgSiO_3$(pv) data. For a given Hugoniot pressure, 50 to 75% of the overall density spread is attributable to the uncertain-

ties in K_o and $\partial K/\partial P$. Obviously, further refinement of these parameters, especially K/ P, is of great interest for more rigorously comparing our hpp shock-wave data with extrapolations of static compression, ultrasonic, and Brillouin scattering data.

Given uncertainties in the EOS data, we conclude that, at present, the two computed forsterite Hugoniots are essentially identical, as noted earlier by Anderson [1977] and Yagi et al. [1978]. The preferred curves are in excellent agreement with the b-axis data of Jackson and Ahrens. The present a- and c-axis data are 0.15-0.20 g/cm^3 less dense than the theoretical Hugoniots, but still within the range of uncertainty, so neither mixed-oxide nor perovskite-structure assemblages can be excluded as explanations for the new data. We note that there is no need to invoke phase changes to forms denser than the perovskite structure to explain the forsterite data. This conclusion is supported by shock-wave work on enstatite [J. P. Watt and T. J. Ahrens, manuscript in preparation, 1983].

We have fitted Hugoniots through the a- and c-axis data and data at pressures above 90 GPa of Syono et al.[1981a], McQueen [1968], Marsh [1980] and Jackson and Ahrens [1979], excluding the four highest b-axis data, to estimate K_o and $\partial K/\partial P$ values required by these lower compressibility data. With γ_o, n, and E_{tr} fixed at the preferred values in Table 2, we find that K_o and $\partial K/\partial P$ are 207 GPa and 5.2, respectively, for oxides (ρ_o = 3.86 g/cm^3) and 253 GPa and 4.6, respectively, for a pv assemblage (ρ_o=3.94 g/cm^3) for the 10 data points used in the fit. These values are by no means unreasonable. On the other hand, assuming that all the high-pressure phase equation of state parameters, except zero-pressure density, for the a- and c-axis samples are the same as the preferred values for a perovskite-structure assemblage (Table 2), we can find ρ_o of the high-pressure phase needed to satisfy the a- and c-axis data. We calculate a ρ_o of 3.77 g/cm^3 compared to the value of 3.94 g/cm^3 needed to satisfy the b axis data and calculated from static compression results. Thus the "average" zero-pressure density of the high-pressure phase of shock-loaded forsterite is between 3.80 and 3.90 g/cm^3 and is less than one would expect for an MgO + $MgSiO_3$(pv) assemblage. The uncertainties in the equation of state parameters, however, do not necessarily require such a lowered density.

We can estimate a high-pressure phase Hugoniot of polycrystalline forsterite from the a-, b-, and c-axis data by using the following simple approach. If we consider polycrystalline forsterite as a random mixture of single crystals with the three axes represented in statistically equal amounts, the average Hugoniot of the mixture can be computed from the mass fraction weighted Hugoniot densities of the three "components" [Ahrens et al., 1977]. This method has been shown to reproduce the Hugoniots of rocks whose mineral components have been well characterized under shock, for example, Westerly granite. Since the a- and c-axis Hugoniot densities are virtually equal, we can write an "average" polycrystalline density $\langle\rho\rangle$ at a given pressure as

$$\langle\rho\rangle = 3[2/\rho(a,c) + 1/\rho(b)]^{-1} \quad (1)$$

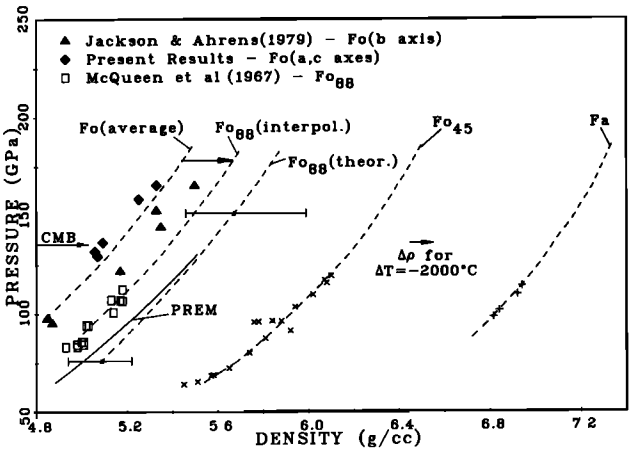

Fig. 4. Summary of shock compression data for olivines. Fo_{88} curve is a linear interpolation between the "average" Fo_{100} curve and Fa. Data for Fo_{45} and Fa are from McQueen and Marsh[1966], McQueen et al. [1967], and Marsh [1980]. Also shown is a theoretical Hugoniot for Fo_{88} calculated from third-order finite strain and ultrasonic and static compression equation of state parameters. The Parametric Reference Earth Model (PREM) is given to the core-mantle boundary (CMB). The line labelled $\Delta\rho$ represents the density increase for a reduction in temperature of 2000°K from the CMB Hugoniot to lower mantle temperatures.

where $\rho(x)$ is the Hugoniot density of the x axis. We plot our calculated $\langle\rho\rangle$ in Figure 3 and conclude that polycrystalline forsterite should, on average, shock load to densities lower than those of the preferred theoretical Hugoniots. Note that the dense polycrystal data of McQueen [1968] and Marsh [1980] at pressures around 100 GPa are consistent with this conclusion, thus giving confidence in Hugoniot data obtained from dense polycrystals. We emphasize that this averaging method is simplistic, but given the errors in the experimental data, more rigorous averaging treatments are not warranted.

We estimate the bulk modulus and its pressure derivative of the high-pressure phase of forsterite by combining our "average" polycrystalline Hugoniot with dense polycrystal data of McQueen [1968] and Marsh[1980] at pressures above 90 GPa. Keeping n, γ_o, and E_{tr} fixed at their values in Table 2, we find that varying the zero-pressure density of the high-pressure phase from 3.6 to 3.8 g/cm^3, the bulk modulus increases from 141 to 217 GPa, and its first pressure derivative decreases from 4.9 to 4.0.

We now compare the forsterite single-crystal results with P-ρ values for the lower mantle derived from inversion of normal mode and seismic travel time data. In Figure 4, we plot the Hugoniot data for single-crystal forsterite, Fo, for the three orthorhombic axes. We also include data of McQueen and Marsh [1966] and Marsh [1980] for fayalite, Fa, (Rockport, Massachusetts, ρ= 4.28, compared to 4.38 for stoichiometric fayalite), Fo_{45}(dunite, Mooihoek Mine, Transvaal [McQueen et al., 1967]), and Fa_{12}(dunite, Twin Sisters Peaks, Washington [McQueen et al., 1967]). Note that Jackson and Ahrens [1979] incorrectly take Twin

Sisters dunite composition as Fo_{92} rather than Fo_{88} [Birch, 1960]. We plot pressure vs. density for the Preliminary Reference Earth Model (PREM) [Dziewonski and Anderson, 1981] in the lower mantle to the core-mantle boundary (CMB).

We calculate Hugoniots for Fo_{88} by linear interpolation between the Fo_{100} and Fa data in Figure 4 to compare with both Twin Sisters dunite and the lower mantle. For Fo_{100}, we use our "average" Fo_{100} Hugoniot. The striking linearity of shock properties of olivines with iron content is apparent from the fact that interpolation between the forsterite single-crystal data and the Fo_{45} data yields virtually the same Fo_{88} Hugoniot (to within 0.01 g/cm^3) as does interpolation between Fo and Fa. The interpolated Fo_{88} Hugoniot is in excellent agreement with the Twin Sisters dunite data. If the a- and c-axis Fo_{100} data and the b-axis Fo_{100} data are used separately, the interpolated Fo_{88} curves closely bracket the Twin Sisters dunite data. Note that interpolation using only the b-axis data overestimates Twin Sisters densities. The Twin Sisters dunite data have previously not been well fit by "systematics" [see Jackson and Ahrens, 1979].

We include in Figure 4 a theoretical Hugoniot for Fo_{88} calculated from the preferred EOS parameters for a perovskite-structure assemblage. The error bars include the combined uncertainties in K_o and $\partial K/\partial P$. The theoretical Hugoniot yields higher densities than are found experimentally, although the observed data are marginally compatible with the range of theoretical densities. More static compression studies of perovskite-structure silicates, particularly investigations of K_o and $\partial K/\partial P$, are needed to determine whether the apparent discrepancy between computed and observed olivine Hugoniots is real.

The present results do not suggest a need for "post-perovskite" phases of olivines as proposed by Jeanloz and Ahrens [1977] and Jackson and Ahrens [1979]. Indeed, they offer only marginal evidence for formation of perovskite-structure high-pressure products.

Finally, we compare experimental results for shock-compressed olivines with the lower mantle density of seismic earth model PREM. We note that temperatures reached in shock-wave experiments at pressures comparable to lower mantle pressures are higher than estimated lower mantle temperatures. For example, Stacey [1977] calculated a temperature of 3157°K at the core-mantle boundary (P = 135 GPa). Brown and Shankland [1981] found a value of 2449°K for an adiabatic mantle; a superadiabatic contribution estimated at 200°K would raise the CMB temperature to 2650°K. Lyzenga and Ahrens [1980] measured shock temperature in three forsterite single crystals shocked between 150 and 180 GPa and combining their data and the forsterite Hugoniot temperature calculations of Ahrens et al. [1969], found shock temperatures of 3800±750°K at 135 GPa. Thus shock temperatures at 135 GPa (the base of the mantle) are 400-1900°K higher than those estimated in the Earth. The shock densities are consequently lower than would occur in the Earth. Correcting Hugoniot densities for this temperature effect would increase the measured densities by no more than 0.10 g/cm^3 for a difference of 2000°K.

Taking this maximum density correction into account, we find that PREM and our interpolated Fo_{88} density curves are compatible. In fact, olivine compositions of as low as Fo_{80} are permitted by the a- and c-axis Hugoniot data, assuming minimum values for olivine shock temperatures, and compositions as high as Fo_{89}, from the b-axis data and maximum shock temperatures. These values are lower than Liu's [1977], Watt and O'Connell's [1978], and Watt and Ahrens' [1982] Mg mole fractions of 0.90-0.95 in perovskite-structure olivine and pyroxene lower mantles. These studies were based on static compression data for pv and, as can be seen in Figure 4, lead to higher calculated lower mantle densities and thus higher Mg mole fractions than observed in the shock-wave experiments. If we use the preferred theoretical Fo_{88} curve and the measured Fo_{45} and Fa data, we find that we need a composition between Fo_{91} and Fo_{96}, depending on the size of the temperature correction, to match PREM densities.

Thus, results of shock-wave compression experiments on olivines suggest that the lower mantle has an iron content similar to the upper mantle, where Mg mole fractions range from 0.85 to 0.90, or the lower mantle may be enriched in iron by up to 0.1 Mg mole fraction. This is in contrast to the conclusion of similar, or depleted, lower mantle iron contents reached from consideration of static compression data on olivines and pyroxenes. Obviously, better precision high-pressure studies, especially ones that address thermal properties, of olivines are necessary to resolve this discrepancy.

Table 3 presents the results of the Hugoniot elastic limit experiments. To calculate the elastic state, we use the free-surface approximation, $u_p = u_{fs}/2$, where u_{fs} is the sample free surface velocity determined from reflections from the inclined mirror on top of the sample [Rice et al., 1958]. We ignore interactions among the various waves in the samples; the error in so doing is small [Raikes and Ahrens, 1979]. We also include for comparison the c-axis datum of Raikes and Ahrens [1979] and summaries of the data of Syono et al. [1981a]. In the latter case, we give averages for elastic velocities and elastic states with the number of measurements averaged indicated. In this case, the stated uncertainty is the largest deviation of the individual data points from the calculated average.

The present results are in good agreement with the data of Syono et al. We do not compare deformational states, since these depend on projectile velocity. Elastic states should, however, be comparable. The Hugoniot elastic limits increase for loading along the a, c and b axes, in that order. Elastic (compressional) velocities determined from the shock wave experiments agree with those measured ultrasonically [Graham and Barsch, 1969; Kumazawa and Anderson, 1969]. Ultrasonic velocities are 10.10, 7.88, and 8.55 km/sec for propagation along the a, b, and c axes, respectively.

We find more complex behavior at low pressures than has been previously reported for shock loading along the a axis. Our b-axis streak record is very similar to that observed by Raikes and Ahrens [1979] for loading along the c axis, an elastic shock followed by a single deformational shock wave. Figure 5 shows static and streak records for loading along the a axis (shot 515). The

TABLE 3. Single-Crystal Forsterite Elastic and Deformational States

Shot	ρ_o, g/cm^3	u_{fp}, km/s	u_e, km/s	u_s, km/s	Elastic state u_p, km/s	Elastic state P, GPa	Elastic state ρ, g/cm^3	Deformational state u_p, km/s	Deformational state P, GPa	Deformational state ρ, g/cm^3
a-axis										
515	3.2257 (±0.0021)	1.56 (±0.01)	10.13 (±0.07)	7.54 (±0.07)	0.16 (±0.01)	5.2 (±0.4)	3.28 (±0.01)	0.39 (±0.01)	9.6 (±0.3)	3.46 (±0.01)
				6.63 (±0.06)				0.67 (±0.01)	16.1 (±0.1)	3.62 (±0.01)
530	3.2259 (±0.0021)	1.75 (±0.01)	9.54 (±0.06)	7.28 (±0.06)	0.21 (±0.01)	6.6 (±0.1)	3.30 (±0.01)	0.37 (±0.01)	8.8 (±0.3)	3.48 (±0.03)
				6.90 (±0.06)				0.76 (±0.01)	18.3 (±0.2)	3.70 (±0.03)
Syono et al. (4 shots)		-	10.27 (±0.09)	-	0.20 (±0.02)	6.5 (±0.5)	3.29 (±0.01)	-	-	-
b-axis										
503	3.2222 (±0.0014)	1.68 (±0.01)	8.37 (±0.04)	6.52 (±0.04)	0.45 (±0.01)	12.1 (±0.4)	3.40 (±0.01)	0.71 (±0.01)	17.9 (±0.2)	3.56 (±0.01)
Syono et al. (2 shots)		-	8.57 (±0.12)	-	0.45 (±0.01)	12.3 (±0.3)	3.40 (±0.00)	-	-	-
c-axis										
Raikes and Ahrens		-	8.72 (±0.07)	-	0.31 (±0.02)	8.7 (±0.7)	3.33 (±0.01)	-	-	-
Syono et al. (6 shots)		-	8.94 (±0.22)	-	0.32 (±0.06)	9.1 (±2.4)	3.34 (±0.03)	-	-	-

u_e is elastic wave velocity; other designations are the same as in Table 1.

inclined mirror image cannot be explained by an elastic shock followed by a single deformational shock; instead, we require three distinct shocks to accommodate the two breaks in the inclined mirror image. Moreover, three shock fronts are clearly discernible on the two flat arrival mirrors on the upper specimen surface. A similar complex structure was observed when the a-axis experiment was repeated (shot 530). Both shock states are included in Table 3. The elastic shock state, of amplitude 5.9±0.7 GPa, is followed by a second shock of 9.2±0.4 GPa amplitude. The third shock amplitude was 17.1±1.1 GPa. Syono et al. do not describe such a structure in their four a-axis experiments, possibly because their measurements were made at higher projectile velocities (2.0-3.8 km/sec) than the 1.6-1.8 km/s range of the present experiments. Figure 1 of Syono et al. [1981a], a streak record for an a-axis experiment appears to exhibit some curvature in the region between labels t_1 and t_2, and thus may be similar to that in Figure 20 of Ahrens and Gregson [1964] for Solenhofen limestone and attributed by them to nonequilibrium states between the HEL and the final, stable shock state.

Another explanation could be that the second, intermediate shock front represents the forsterite $\alpha \rightarrow \beta$ or γ transition that has not been previously observed under shock loading. Calculation of temperature on the forsterite Hugoniot at 10 GPa using a Grüneisen parameter of 1.13 [Graham and Barsch, 1969; Kumazawa and Anderson, 1969] gives a value of no more than 50°C. Extrapolation of the static compression $\alpha \rightarrow \beta$ phase boundary of Suito [1977] to 50°C yields a transition pressure of 11 GPa, while the phase boundary of Ito et al.[1971] extrapolates to 6 GPa. Extrapolation of Suito's [1977] $\beta \rightarrow \gamma$ phase boundary to 50°C produces a transition pressure of 11.8 GPa. These estimates compare to a pressure of 9-10 GPa found for the second shock in our experiments. Thus the observed pressure is compatible with that expected for the $\alpha \rightarrow \beta$ or γ transformation occurring at low temperatures.

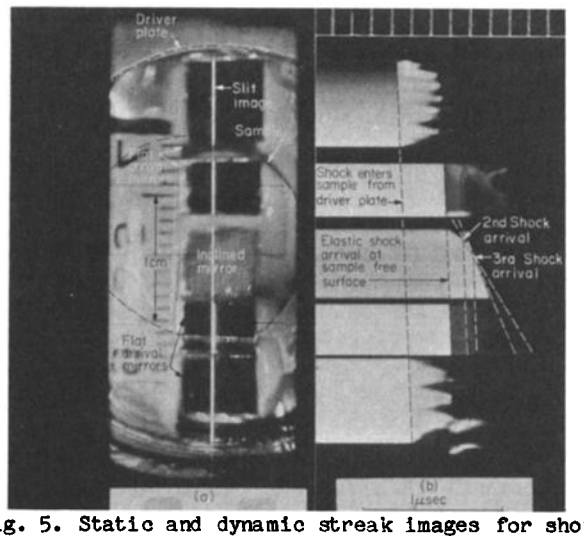

Fig. 5. Static and dynamic streak images for shot 515 upon shock compression to 16 GPa along the a axis of single-crystal forsterite. (a) Static image as seen through streak camera. (b) Streak image showing three-wave structure recorded by inclined mirror and flat arrival mirrors.

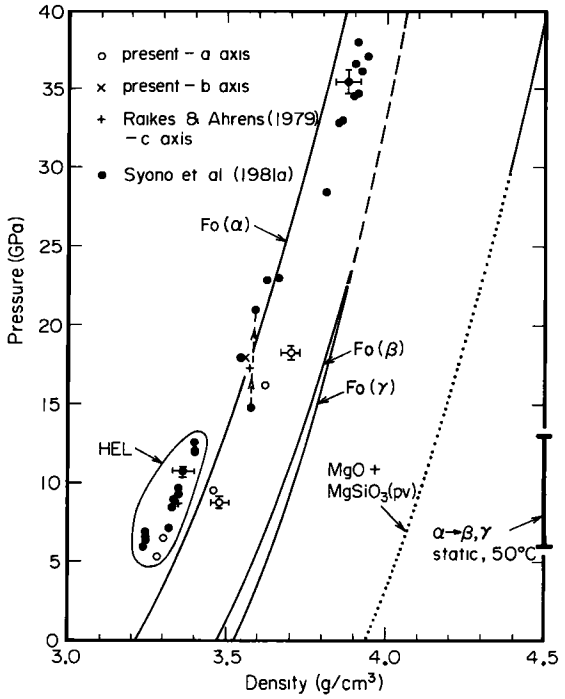

Fig. 6. Experimental Hugoniot data for single-crystal forsterite for pressures up to 40 GPa and computed Hugoniots for the α, β, and γ phases of forsterite and for a perovskite-structure high-pressure assemblage. The pressure range at which the $\alpha \rightarrow \beta$ or γ transformation could occur at static conditions (extrapolated to 50-100°C) is shown. HEL denotes the Hugoniot elastic limit.

In Figure 6 we plot the present data for the a- and b-axis shots, the c-axis data of Raikes and Ahrens [1979], and that of Syono et al. [1981a] at Hugoniot pressures below 40 GPa. We include typical errors for the Syono et al. data. Also shown are theoretical Hugoniots calculated for α, β, and γ phases of forsterite from the equation of state data collected by Jeanloz and Thompson [1983]. The data of Syono et al. and the b and c axis data are in excellent agreement with the Fo(α) Hugoniot for pressures to 30 GPa; for higher pressures, the measured points are displaced to higher densities. The Syono et al. datum at 15 GPa, below the theoretical Hugoniot, was calculated using the free-surface approximation; the dashed line joins this point to the corresponding point at 21 GPa computed by the impedance matching method. Thus the reliability of the free-surface approximation point is questionable. In all other cases where Syono et al. [1981a] analyzed their data by using both techniques, the calculated Hugoniot pressures below 40 GPa agreed within 1.5 GPa or less. Our a-axis Hugoniot data between 9 and 10 GPa are shifted to higher densities relative to the Fo(α) theoretical Hugoniot, as are the data at 16 and 18 GPa arising from the third shock. Thus the mixed-phase region for loading along the a axis begins at pressures 10-15 GPa lower than for the b and c axes. This strongly suggests that a phase transition is occurring in the forsterite samples

shocked along the a axis. It is unlikely that this represents the onset of the MgO + $MgSiO_3$(pv) transition that occurs at about 27 GPa under static conditions, extrapolated to 50°C from data of Ito and Yamada [1982], and we conclude that our a-axis data may represent the $\alpha \rightarrow \beta$ or γ transition in forsterite. The density increase at 9 GPa is 1-2% compared to the 6-8% increase needed for complete transformation to the β or γ form. We note that because of the very similar β and γ Hugoniots, it will likely not be possible to distinguish between the two phases in shock experiments if our a-axis observation is confirmed to represent a phase transformation.

Two possible problems with this explanation are the question of whether the transition kinetics are such as to allow the transformation to occur over the short duration of shock loading and the fact that many transformations that have been observed under shock require considerable pressure overdriving compared to static experiments. Moreover, the hypothesis that the onset of a shock-induced phase change occurs at about 9 GPa implies that the Hugoniot represents an equilibrium phase assemblage more closely than has heretofore been assumed. Poirier [1981] modelled the $\alpha \rightarrow \beta$ transition in terms of propagating partial dislocations, and his results would seem to indicate that the transition could not occur at the conditions of the shock experiments. Obviously, this new observation of what appears to be a transition shock wave in forsterite compressed along the a axis merits further investigation.

Conclusions

We report dynamic compression results for single-crystal forsterite shocked along the a and c axes for comparison with b-axis data of Jackson and Ahrens [1979]. Our a- and c-axis results are displaced to lower particle velocity in u_s-u_p space relative to the data for the b axis. The a- and c-axis data form a single straight line parallel to the straight line for the b-axis values. In P-ρ space, the a- and c-axis velocity offset leads to a displacement of the Hugoniot to lower densities compared to the b-axis Hugoniot indicating that single-crystal forsterite is most compressible along the b axis. This observation disagrees with the prediction of maximum compression along the a axis from the crystallographically-based model of Jeanloz [1980] that does not invoke phase transitions to account for the high-pressure dynamic behavior of forsterite.

These data represent the highest pressures for which directional dependence of dynamic behavior has been found. Directional dependence has been reported previously for much lower pressures for single-crystal calcite, ilmenite and sodium chloride. The extensive single-crystal results of Syono et al. [1981a] to pressures of 92 GPa exhibit slightly higher densities for compression of the b axis in agreement with the present results, although estimated errors in the lower pressure data do not allow an unambiguous conclusion to be reached when the data are examined independently of the present data.

We have compared our Hugoniot data with theoretical Hugoniots for mixed-oxide and perovskite-structure assemblages of forsterite constructed using recent static compression, ultrasonic, and Brillouin scattering data. We find that the high-pressure Hugoniots of mixed-oxide and perovskite-structure assemblages are nearly indistinguishable and are in excellent agreement with the data of Jackson and Ahrens [1979] for the b axis. Thus we do not require transformation to structures denser than oxides or perovskites to explain the shock-wave data. The a- and c- axis data are less dense than the calculated Hugoniots by 0.15-0.20 g/cm^3, but lie within the range of Hugoniots produced by the combined uncertainties in the equation of state data. From 50 to 70% of the overall uncertainty is caused by the uncertainty in K_o and $\partial K/\partial P$, so that refinement of these values is of great interest, especially for $MgSiO_3$(pv).

Least squares fits to the data for the a and c axes with ρ_o fixed at values appropriate for mixed-oxide and perovskite assemblages yield K_o and $\partial K/\partial P$ values of 207 GPa and 5.2, respectively, for oxides and 253 GPa and 4.6 respectively, for a pv assemblage. We have estimated a zero-pressure density of the high-pressure phase of the a- and c-axis shock-loaded forsterite of 3.77 g/cm^3, assuming the preferred values of the other equation of state parameters for a perrovskite-structure assemblage, compared with 3.94 g/cm^3 calculated from static compression data. The latter value is consistent with the b-axis data.

A simple averaging calculation (mass fraction weighted addition of individual axis Hugoniots) gives an "average" forsterite Hugoniot about 0.13 g/cm^3 less dense than the preferred theoretical Hugoniots, in agreement with data on dense polycrystalline forsterite to 100 GPa.

Partial release paths for the a-axis experiments are very steep and are comparable to those reported by Jackson and Ahrens [1979] along the b axis. The c-axis release paths are much shallower suggesting that the samples revert to their low-pressure form rapidly upon unloading. The fact that shock compression of the a and c axes produces similar Hugoniot states, but markedly different release states is further evidence for a complex shock process in single-crystal forsterite.

We have compared shock-wave data for single-crystal forsterite with the PREM density profile in the lower mantle. Interpolated Hugoniots for Fo_{88} based on the Fo_{100} single-crystal data and previous data of McQueen et al. [1967] and Marsh [1980] for Fo_{45} and Fa bracket the Hugoniot data of McQueen et al. [1967] for Twin Sisters dunite (Fo_{88}), suggesting a highly linear variation of olivine Hugoniots with iron content. Considering differences between shock temperatures and lower mantle temperature estimates, we conclude that an olivine stoichiometry lower mantle with Mg mole fraction between 0.80 and 0.89 is compatible with PREM densities. These values are lower than the Mg mole fraction estimates of 0.90 to 0.95 of Liu [1977], Watt and O'Connell [1978], and Watt and Ahrens [1982], from extrapolation of static compression results for perovskite-structure olivine and pyroxene. This disagreement demonstrates the importance of further research on the properties of olivine and pyroxene stoichiometries at lower mantle conditions.

In three a- and b-axis experiments at impact velocities lower than have been previously used on single-crystal forsterite, we have observed a two-wave (elastic and deformational) structure

for the b axis very similar to that of Raikes and Ahrens [1979] for the c axis; however, for the a axis, we find a three-wave (elastic and two deformational) structure. The Hugoniot elastic limits we determine are in excellent agreement with the results of Syono et al.[1981a]; however, they did not observe the complex wave structure found here, perhaps because their experiments were made at somewhat higher impact velocities. The pressure at which the first shock wave is observed is about 9 GPa, in approximate agreement with the pressure at which the forsterite $\alpha \rightarrow \beta$ or γ transition occurs under static conditions. This shock state and that determined from the second shock wave at 16-18 GPa are displaced to densities higher than those for the computed Fo(α) Hugoniot by 0.05-0.15 g/cm^3. Thus, the mixed-phase region begins at lower pressure for the a axis than for the b and c axes. The Hugoniot temperature is only about 350°K, which may indicate that the transition is not thermally activated and occurs on the short time scale of shock experiments based on a dislocation model for the transition [Poirier, 1981]. More detailed study of this apparent phase transition front is warranted.

Acknowledgments. We appreciate the careful construction and execution of these experiments by E. Gelle and M. Long and acknowledge useful discussions with G. A. Lyzenga and J. M. Vizgirda. D. L. Anderson offered helpful comments on the manuscript. We are again grateful to T. J. Shankland for providing these crystals to us. Computing support was provided by the Office of Computer Services and the Department of Geology, Rensselaer Polytechnic Institute. Supported by NSF grant EAR 80-18819. Contribution 3809, Division of Geological and Planetary Sciences, California Institute of Technology.

References

Ahrens, T. J., and V. G. Gregson, Shock compression of crustal rocks: Data for quartz, calcite and plagioclase rocks, J. Geophys. Res., 69, 4839-4874, 1964.

Ahrens, T. J., and C. F. Petersen, Shock wave data and the study of the Earth, in The Application of Modern Physics to the Earth and Planetary Interiors, edited by S. K. Runcorn, pp. 449-461, John Wiley, New York, 1969.

Ahrens, T. J., W. H. Gust, and E. B. Royce, Material strength effect in the shock compression of alumina, J. Appl. Phys., 39, 4610-4616, 1968.

Ahrens, T. J., D. L. Anderson, and A. E. Ringwood, Equations of state and crystal structures of high-pressure phases of shocked silicates and oxides, Rev. Geophys. Space. Phys., 7, 667-707, 1969.

Ahrens, T. J., J. H. Lower, and P. L. Lagus, Equation of state of forsterite, J. Geophys. Res., 76, 518-528, 1971.

Ahrens, T. J., I. Jackson, and R. Jeanloz, Shock compression and adiabatic release of a titaniferous basalt, Proc. Lunar. Sci. Conf., 8th, 3437-3455, 1977.

Anderson, D. L., Petrology of the mantle, Mineral. Soc. Am. Spec. Pap., 3, 85-95, 1970.

Anderson, D. L., Composition of the mantle and core, Annu. Rev. Earth Planet. Sci., 5, 179-202, 1977.

Anderson, D. L., C. Sammis, and T. Jordan, Composition and evolution of the mantle and core, Science, 171, 1103-1112, 1971.

Anderson, O. L., and P. Andreatch, Pressure derivatives of elastic constants of single-crystal MgO at 23° and -195.8°C, J. Am. Ceram. Soc., 49, 404-409, 1966.

Bass, J. D., R. C. Liebermann, D. J. Weidner, and S. J. Finch, Elastic properties from acoustic and volume compression experiments, Phys. Earth Planet. Inter., 25, 140-158, 1981.

Birch, F., Elasticity and constitution of the Earth's interior, J. Geophys. Res., 57, 227-286, 1952.

Birch, F., The velocity of compressional waves in rocks to 10 kilobars, 1, J. Geophys. Res., 65, 1083-1102, 1960.

Brown, J. M., and T. J. Shankland, Thermodynamic parameters in the Earth as determined from seismic profiles, Geophys. J. R. Astron. Soc., 66, 579-596, 1981.

Burdick, L., and D. L. Anderson, Interpretation of velocity profiles of the mantle, J. Geophys. Res., 80, 1070-1074, 1975.

Butler, R., and D. L. Anderson, Equation of state fits to the lower mantle, Phys. Earth Planet. Inter., 17, 147-162, 1978.

Chang, E., and E. K. Graham, The elastic constants of cassiterite SnO_2 and their pressure and temperature dependence, J. Geophys. Res., 80, 2595-2599, 1975.

Dandekar, D. P., and A. L. Ruoff, Temperature dependence of the elastic constants of calcite between 160° and 300°K, J. Appl. Phys., 39, 6004-6009, 1968.

Davies, G. F., Limits on the constitution of the lower mantle, Geophys. J. R. Astron. Soc., 38, 479-503, 1974.

Dziewonski, A. M., and D. L. Anderson, Preliminary reference Earth model, Phys. Earth Planet. Inter., 25, 297-356, 1981.

Fritz, J. N., S. P. Marsh, W. J. Carter, and R. G. McQueen, The Hugoniot equation of state of sodium chloride in the sodium chloride structure, NBS Spec. Publ., 326, 201-208, 1971.

Gaffney, E. S., and D. L. Anderson, Effect of low spin Fe^{2+} on the composition of the lower mantle, J. Geophys. Res., 78, 7005-7014, 1973.

Graham, E. K., and G. R. Barsch, Elastic constants of single-crystal forsterite as a function of temperature and pressure, J. Geophys. Res., 74, 5949-5960, 1969.

Ito, E., The absence of oxide mixture in high-pressure phases of Mg-silicates, Geophys. Res. Lett., 4, 72-74, 1977.

Ito, E., and H. Yamada, Stability relations of silicate spinels, ilmenites, and perovskites, in High Pressure Research in Geophysics, edited by S. I. Akimoto and M. H. Manghnani, pp. 405-419, Center for Academic Publications, Tokyo, 1982.

Ito, K., S. Endo, and N. Kawai, Olivine-spinel transformation in a natural forsterite, Phys. Earth Planet. Int., 4, 425-428, 1971.

Jackson, I., and T. J. Ahrens, Shock wave compression of single-crystal forsterite, J. Geophys. Res., 84, 3039-3048, 1979.

Jackson, I., and H. Niesler, The elasticity of periclase to 3 GPa and some geophysical implications, in High Pressure Research in Geophysics, edited by S. I. Akimoto and M. H. Mangh-

nani, pp. 93-113, Center for Academic Publications, Tokyo, 1982.

Jakubith, M., and P. Seidel, Shock-loading experiments on eclogite, Geophys. Res. Lett., 9, 408-411, 1982.

Jeanloz, R., Shock effects in olivine and implications for Hugoniot data, J. Geophys. Res., 85, 3163-3176, 1980.

Jeanloz, R., and T. J. Ahrens, Pyroxenes and olivines: Structural implications of shock-wave data for high-pressure phases, in High-Pressure Research: Applications in Geophysics, edited by M. H. Manghnani and S. Akimoto, pp. 439-461, Academic, New York, 1977.

Jeanolz, R., and T. J. Ahrens, Release adiabat measurements on minerals: The effect of viscosity, J. Geophys. Res., 84, 7545-7548, 1979.

Jeanloz, R., and T. J. Ahrens, Equations of state of FeO and CaO, Geophys. J. R. Astron. Soc., 62, 505-528, 1980.

Jeanloz, R., and A. B. Thompson, Phase transformations and mantle discontinuities, Rev. Geophys. Space Phys., 21, 51-74, 1983.

Jeanloz, R., T. J. Ahrens, J. S. Lally, G. L. Nord, J. M. Christie, and A. H. Heuer, Shock-produced olivine glass: First observation, Science, 197, 457-459, 1977.

King, D. A., and T. J. Ahrens, Shock compression of ilmenite, J. Geophys. Res., 81, 931-935, 1976.

Kumazawa, M., and O. L. Anderson, Elastic moduli, pressure derivatives, and temperature derivatives of single-crystal olivine and single-crystal forsterite, J. Geophys. Res., 74, 5961-5972, 1969.

Liebermann, R. C., L. E. A. Jones, and A. E. Ringwood, Elasticity of aluminate, titanate, stannate, and germanate compounds with the perovskite structure, Phys. Earth Planet. Inter., 14, 165-178, 1977.

Liu, L. G., Post-oxide phases of forsterite and enstatite, Geophys. Res. Lett., 2, 417-419, 1975.

Liu, L. G., The post-spinel phase of forsterite, Nature, 262, 770-772, 1976a.

Liu, L. G., Orthorhombic perovskite phases observed in olivine, pyroxene, and garnet at high pressures and temperatures, Phys. Earth Planet. Inter., 11, 289-298, 1976b.

Liu, L. G., Mineralogy and chemistry of the Earth's lower mantle above 1000 km, Geophys. J. R. Astron. Soc., 48, 53-62, 1977.

Liu, L., W. A. Bassett, and T. Takahashi, Isothermal compression of a spinel phase of Co_2SiO_4 and magnesian ilmenite, J. Geophys. Res., 79, 1171-1174, 1974.

Lyzenga, G. A., and T. J. Ahrens, The relation between the shock-induced free-surface velocity and the postshock specific volume of solids, J. Appl. Phys., 49, 201-204, 1978.

Lyzenga, G. A., and T. J. Ahrens, Shock temperature measurements in Mg_2SiO_4 and SiO_2 at high pressures, Geophys. Res. Lett., 7, 141-144, 1980.

Mao, H. K., T. Yagi, and P. M. Bell, Mineralogy of the Earth's deep mantle: Quenching experiments on mineral compositions at high pressure and temperature, Year Book Carnegie Inst. Washington, 1976, 502-504, 1977.

Marsh, S. P., Shock Hugoniot Data, University of California Press, Berkeley, 1980.

McQueen, R. G., The equation of state of mixtures, alloys, and compounds, in Seismic Coupling, Advanced Research Project Meeting, edited by G. Simmons, pp.53-106, National Technical Information Service, Springfield, Va., 1968.

McQueen, R. G., and S. P. Marsh, in Handbook of Physical Constants, Mem. 97, edited by S. P. Clark, pp. 153-159, Geological Society of America, Boulder, Colo., 1966.

McQueen, R. G., S. P. Marsh, and J. N. Fritz, Hugoniot equation of state of twelve rocks, J. Geophys. Res., 72, 4999-5036, 1967.

McQueen, R. G., S. P. Marsh, J. W. Taylor, J. N. Fritz, and W. J. Carter, The equation of state of solids from shock wave studies, in High Velocity Impact Phenomena, edited by R. Kinslow, pp. 294-419 and appendices, Academic, New York, 1970.

Poirier, J. P., On the kinetics of olivine-spinel transition, Phys. Earth Planet. Inter., 26, 179-187, 1981.

Raikes, S. A., and T. J. Ahrens, Post-shock temperatures in minerals, Geophys. J. R. Astron. Soc., 58, 717-748, 1979.

Rice, M. H., R. G. McQueen, and J. M. Walsh, Compression of solids by strong shock waves, Solid State Phys., 6, 1-63, 1958.

Sawamoto, H., Orthorhombic perovskite $(Mg,Fe)SiO_3$ and the constitution of the lower mantle, in High-Pressure Research: Applications in Geophysics, edited by M. H. Manghnani and S. I. Akimoto, pp. 219-244, Academic, New York, 1977.

Stacey, F. D., A thermal model of the Earth, Phys. Earth Planet. Inter., 15, 341-348, 1977.

Spetzler, H., Equation of state of polycrystalline and single-crystal MgO to 8 kilobars and 800°K, J. Geophys. Res., 75, 2073-2087, 1970.

Suito, K., Phase relations of pure Mg_2SiO_4 up to 200 kilobars, in High-Pressure Research: Applications in Geophysics, edited by M. H. Manghnani and S. I. Akimoto, pp. 255-266, Academic, New York, 1977.

Syono, Y., T. Goto, J.-I. Sato, and H. Takei, Shock compression measurements of single-crystal forsterite in the pressure range 15-93 GPa, J. Geophys. Res., 86, 6181-6186, 1981a.

Syono, Y., T. Goto, H. Takei, M. Tokonami, and K. Nobugai, Dissociation reaction in forsterite under shock compression, Science, 214, 177-179, 1981b.

Trunin, R. F., V. I. Gon'shakova, G. V. Simakov, and N. E. Galdin, A study of rocks under the high pressures and temperatures created by shock compression, Izv. Acad. Sci. USSR Phys. Solid Earth, Engl. Transl., 8, 579-586, 1965.

Vassiliou, M. S., and T. J. Ahrens, Hugoniot equation of state of periclase to 200 GPa, Geophys. Res. Lett., 8, 729-732, 1981.

Wackerle, J., Shock-wave compression of quartz, J. Appl. Phys., 33, 922-937, 1962.

Watt, J. P., and T. J. Ahrens, The role of iron partitioning in mantle composition, evolution, and scale of convection, J. Geophys. Res., 87, 5631-5644, 1982.

Watt, J. P., and R. J. O'Connell, Mixed-oxide and perovskite-structure model mantles from 700-1200 km, Geophys. J. R. Astron. Soc., 54, 601-630, 1978.

Watt, J. P., and L. Peselnick, Clarification of the Hashin-Shtrikman bounds on the effective elastic moduli of polycrystals with hexagonal,

trigonal, and tetragonal symmetries, J. Appl. Phys., 51, 1525-1531, 1980.

Weidner, D. J., J. D. Bass, A. E. Ringwood, and W. Sinclair, The single-crystal elastic moduli of stishovite, J. Geophys. Res., 87, 4740-4746, 1982.

Yagi, T., H. K. Mao, and P. M. Bell, Isothermal compression of perovskite-type $MgSiO_3$, Year Book Carnegie Inst. Washington, 1977, 835-837, 1978.

Yagi, T., H. K. Mao, and P. M. Bell, Lattice parameters and specific volume for the perovskite phase of orthopyroxene composition $(Mg,Fe)SiO_3$, in Year Book Carnegie Inst. Washington, 1978, 612-613, 1979a.

Yagi, T., H. K. Mao, and P. M. Bell, Hydrostatic compression of $MgSiO_3$ of perovskite structure, Year Book Carnegie Inst. Washington, 1978, 613-614, 1979b.

T.J.Ahrens, Seismological Laboratory, California Institute of Technology, Pasadena, CA 91125.

J.P.Watt, Department of Geology, Rensselaer Polytechnic Institute, Troy, NY 12181.

(Received September 23, 1982;
revised June 2, 1983;
accepted, June 16, 1983.)